Contents lists available at: http://qu.edu.iq

Al-Qadisiyah Journal for Engineering Sciences

Journal homepage: https://qjes.qu.edu.iq

Research Paper

Stability analysis of marangoni magneto-convective flow with heat generation: effects of depth ratio and thermal boundaries

Sumithra R. [1], ***Archana M. A.*** [1], ***Manjunatha N.*** [2], ***Khaled Al-Farhany*** [3], ***Shankara*** [4] ***and Vijaya Kumar*** [5]

[1] *Department of Mathematics, Nrupathunga University, Bengaluru, Karnataka, India.*
[2] *Department of Mathematics, School of Applied Sciences, REVA University, Bengaluru, Karnataka, India.*
[3] *Department of Mechanical Engineering, College of Engineering, University of Al-Qadisiyah, Al-Qadisiyah, Iraq.*
[4] *Department of Civil Engineering, Amrita School of Engineering, Amrita Vishwa Vidyapeetham, Bengaluru, India*
[5] *Department of Mathematics, M S Ramaiah Institute of Technology, Bengaluru, Karnataka, India.*

ARTICLE INFO

Article history:
Received 12 April 2025
Received in revised form 02 February 2026
Accepted 17 May 2026

keyword:
Marangoni convection
Two-regions
Heat source
Magnetic field
Adiabatic and isothermal boundary

ABSTRACT

The stability analysis of Marangoni magneto-convection (MMC) is investigated in a two-layer system consisting of an electrically conductive fluid-saturated porous layer overlain by an identical fluid layer, incorporating variable heat sources and a uniform magnetic field. The upper fluid surface is free, allowing surface-tension-driven convection, while the lower porous boundary is rigid. Two thermal boundary conditions are examined: (i) adiabatic–adiabatic (A–A) and (ii) adiabatic–isothermal (A–I). The governing equations are solved analytically using an exact method to obtain the thermal Marangoni number, an eigenvalue, as a function of depth ratio, Darcy number, Chandrasekhar number, internal Rayleigh numbers, wave number, and thermal diffusivity ratio. Graphical results show that the onset of MMC can be either advanced or delayed by appropriate choices of depth ratio and thermal boundary conditions. The novelty of the present work lies in deriving closed-form expressions for a composite fluid–porous system with simultaneous consideration of variable internal heat sources and magnetic effects under dual thermal boundary conditions, and demonstrating how depth ratio and thermal boundary conditions can be strategically tuned to either advance or delay the onset of instability.

1. Introduction

Marangoni convection refers to fluid motion driven by gradients in surface tension along an interface. These gradients are often induced by internal heat sources and temperature variations. Among the various mechanisms of convective instability, those triggered by internal heating have garnered significant attention due to their relevance in a wide range of engineering and scientific applications. These include nuclear reactor cores, fire dynamics and combustion modelling, crystal growth, post-accident heat removal, welding processes, and beam melting techniques. Convection in a horizontal composite of two or more layers is very significant from a geological standpoint. Examples of this include water reservoirs, thermal circulation in lakes and shallow coastal regions, fibrous and granular thermal insulations, flow in geysers and hot springs. Saghir et al. [1] examined the effects of Rayleigh and Marangoni convection in a dual liquid-porous rectangular cavity system. Their results show that depth ratio governs flow pattern, with suppression of buoyancy effect in the porous layer and enhancement of flow in the fluid layer due to Marangoni convection. Kozak et al. [2] studied the combined effects of thermocapillary and evaporation in a liquid-porous system with lateral heating, showing that the transition of flow from the liquid layer to the porous layer is due to the thickness ratio. Shivakumara et al. [3] analyzed the onset of Darcy-Benard Marangoni convection in an extended Darcy-Brinkman-Forchheimer-Lapwood model with high permeability, both numerically and analytically. It was observed that the effect of buoyancy is destabilizing, while an increase in the permeability parameter delays the onset of convection. McFadden [4] emphasizes the linear stability of horizontal fluid bilayers undergoing phase transitions, highlighting how entropy variations and the dynamics between buoyancy and thermocapillary effects operate under a vertical temperature gradient. Manjunatha et al. [5] examined the effects of various temperature profiles in a composite layer, including linear and parabolic, on Marangoni convection and the stability of the system. This investigation uncovered vital insights into how depth ratio and differing thermal profiles influence convection's onset and the overall stability of the system. Sumithra et al. [6] explore convection under conditions of local thermal non-equilibrium, investigating diverse thermal profiles and their stability effects. The research indicates that model (iii) exhibits higher instability, while model (v) demonstrates significant stability, and model (vi) proves more stable than model (iv) in the context of a composite system. Sumithra and Venkatraman [7] analyze LTNE in convection within a composite layer, assessing stability affected by factors like thermal expansion ratios and diffusivity ratios. Their findings reveal that the critical Rayleigh number decreases with increasing fluid phase thermal expansion and diffusivity ratios, accelerating the onset of convection. They underscore the importance of LTNE effects, particularly for lower values of fluid phase parameters, in destabilizing the system. In practical systems such as welding, crystal growth, thin film processing, and microelectronics, internal heat generation significantly influences the onset of Marangoni convection.

*Corresponding Author.
E-mail address: manjumscmphil@gmail.com ; Tel:(+91) 968-662 3528 (Manjunatha N)

https://doi.org/10.30772/qjes.2026.166109.1780

Nomenclature

A	Ratio of heat capacity	κ_f, κ_m	Thermal diffusivities
a, a_m	Horizontal Wave number	ρ_o	Reference fluid density
D, D_m	Differential operators	ϵ_T	Ratio of thermal diffusivities
Da	Darcy number	μ	Fluid viscosity
d, d_m	Depths of the layer	τ_f, τ_m	Magnetic diffusivity ratios
$\vec{H}$	Magnetic field	ϕ	Porosity
K	Permeability	σ	Surface tension
Ma_T	Thermal Marangoni number	μ_p	Magnetic permeability
Pr_f, Pr_m	Prandtl numbers	ν_m	Magnetic viscosity in the fluid layer
P_f, P_m	Total Pressure	ζ	Depth ratio
Q_f, Q_m	Chandrasekhar numbers	ν_{em}	Effective magnetic viscosity
Q_1, Q_2	Heat sources	Φ_f, Φ_m	Amplitude of perturbed temperatures
R_I, R_{Im}	Internal Rayleigh numbers	β	Porous parameter
T_f, T_m	Temperature	*Subscripts*	
T_o	Interface temperature	f	Fluid layer
$\vec{V}_f, \vec{V}_m$	Velocity vectors	m	Porous layer
W_f, W_m	Vertical Velocities	i	Real numbers

Char and Chiang [8, 9] showed that internal heat generation strongly destabilizes the system, shifting the balance between two instability modes: the thermal mode and the surface tensile mode, and extended the they extended this analysis to include the Coriolis force, revealing that rotation has a stabilizing effect, while internal heat generation remains a destabilizing factor. Mokhtari et al. [10, 11] investigated the stability characteristics of Marangoni convection in a Darcy-Brinkman porous medium with internal heat generation. It was observed that internal heat generation destabilizes the porous media, and the onset of Marangoni convection starts earlier. This work was expanded to a two-layer fluid–porous system by employing the Forchheimer extended Darcy model and a deformable free upper boundary, observing that the dimensionless heat strength parameter destabilizes the system. Further, Shivakumara et al. [12] added anisotropy effects, showing that mechanical anisotropy speeds up convection, thermal anisotropy slows it down. Gangadharaiah [13] examines the stability of Darcy–Benard-Marangoni ferroconvection in a horizontal ferrofluid-saturated porous layer, emphasizing the implications of internal heat generation. It reveals that stability is dictated by the dimensionless strength of the internal heat source, the permeability parameter, and the effective viscosity to fluid viscosity ratio. Sumithra et al. [14] studied Marangoni convection in a composite fluid-porous system in the presence of temperature-dependent heat sources, and showed that the internal Rayleigh numbers and Darcy number destabilize the system. Manjunatha et al. [15] examine non-Darcy Three-Component Marangoni convection in a two-layer configuration, concentrating on stability under Adiabatic-Adiabatic and Adiabatic-Isothermal thermal boundary conditions. The study highlights the influence of heat sources/sinks and magnetic fields on thermal Marangoni numbers, providing analytical formulations and graphical illustrations of their effects on stability within fluid-layer-dominant two-layer systems. When the fluid is electrically conducting, the magnetic field influence on convective instability becomes dominant. Chandrasekhar [16] was the first to document this. Rudraiah and Sekhar[17] used a higher-order Galerkin approach to identify the condition for the onset of steady convection in a horizontal magnetic fluid layer with internal heat sources (sinks). Wilson [18] investigated the effect of a uniform vertical magnetic field on Marangoni flow in a liquid layer with a free upper surface. Liu and Wang [19] explore the linear instability of Marangoni-Bénard convection in both single and dual-layer liquid configurations under high-frequency vibrations, emphasizing the shift from stability to instability as the angle between the vibration axis and the horizontal interface is increased. Banjer and Abdullah [20] investigated thermal convection in a two-layer system consisting of a fluid layer above a porous medium under the influence of a vertical magnetic field. Their study focused on the onset of convection, which exhibits bimodal behavior depending on the relative depths of the layers and the strength of the magnetic field. Tagawa [21] delves into the linear stability aspects of Bénard-Marangoni convection within a diamagnetic liquid layer, particularly encircling a cylinder free from gravitational effects. Celli et al. [22] centre their research on the linear stability of Darcy flow in a horizontally oriented channel heated from beneath, meticulously examining the initiation of thermal convection through convective instability. They analysed a steady-state solution that incorporates a pressure gradient alongside buoyancy forces. It scrutinizes how a magnetic field and surface tension interplay to influence convection dynamics. Lyubimova and Parshakova [23] investigate the stability of a conductive state in a two-layer system of immiscible fluids under a constant heat flux, analyzing the initiation of convection influenced by the ratio of layer thickness and gravitational levels. The study identifies long-wave instability modes and their responses to various perturbations, particularly under terrestrial and microgravity environments. Bhavya and Nanjundappa [24] examine the stability of Bénard-Marangoni ferrothermal convection in a ferrofluid-saturated porous layer, concentrating on energy-driven volumetric internal heating. It investigates the modified critical Rayleigh number and the dimensions of convection cells in relation to the heat source's intensity. Results reveal that an increase in internal heat source correlates with a decrease in critical Rayleigh number, resulting in system destabilization, while convection cell sizes become more confined. Yellamma et al. [25] conducted a stability examination of Marangoni convection incorporating heat generation within a two-layer framework, uncovering that the inverted parabolic temperature distribution stands as the most stable, whereas the linear configuration exhibits the highest level of instability. The outcomes underscore conditions leading to instability driven by heating from above or below. Boeck [26] centres on the stability assessment of wall-adhered Benard-Marangoni convection in a vertical magnetic field. The results suggest that the magnetic field increases the convective threshold and confines the least stable modes adjacent to the side walls. Fadzil and Ibrahim [27] investigate oscillatory convection with heat generation, although it does not delve into convection or a dual-layer setup. Using classical linear stability theory, it assesses the onset of convection in a horizontal fluid layer, spotlighting the impact of internal heat generation on the Rayleigh number. Moussa [28] investigates the stability of ferrofluid within a heterogeneous porous medium subjected to a vertical magnetic field. By employing linear stability analysis, it formulates an ordinary differential equation, unveiling that the transition of the wave number is interconnected with both the Peclet number and magnetic characteristics. Most existing studies on Marangoni convection primarily focus on single-layer configurations, while comparatively fewer investigations address composite fluid–porous systems. In addition, many works examine either magnetic effects or internal heat generation separately, with limited attention given to their simultaneous influence on stability characteristics. Exact analytical solutions for such coupled systems are also scarce, as the majority of studies rely on numerical or approximate methods. Furthermore, systematic comparisons between adiabatic–adiabatic (A–A) and adiabatic–isothermal (A–I) thermal boundary conditions in the context of Marangoni magneto-convection within two-layer composite systems remain limited. These gaps highlight the need for a unified analytical treatment that incorporates magnetic effects, variable internal heat sources, and dual thermal boundary conditions within a composite configuration.

2. Mathematical analysis

A system comprising of an isotropic saturated porous region of depth d_m overlying the same fluid of depth d is considered, Fig. 1. A rigid-free velocity at the surfaces with A-A and A-I temperatures is studied. A frame of reference (x, y, z) with the z-axis directing vertically upwards and origin at the meniscus is assumed. The temperatures of the upper and lower boundaries are T_l and T_u with $T_u < T_l$. A uniform magnetic field $\vec{H}$ is applied in the vertical direction as shown in the Fig. 1. The equations of motion governing the above system are listed below [25, 26].

2.1 Fluid layer

In the fluid layer, i.e, $z \in (0, d)$, Eq. 1 up to Eq. 5.

$$\nabla . \vec{V}_f = 0 \tag{1}$$

$$\nabla.\vec{H} = 0 \tag{2}$$

$$\rho_o\left[\frac{\partial\vec{V}_f}{\partial t} + \left(\vec{V}_f.\nabla\right)\vec{V}_f\right] = -\nabla P_f + \mu\nabla^2\vec{V}_f + \mu_p\left(\vec{H}.\nabla\right)\vec{H} \tag{3}$$

$$\left[\frac{\partial T_f}{\partial t} + \left(\vec{V}_f.\nabla\right)T_f\right] = \kappa_f\nabla^2 T_f + Q_1\left(T_f - T_o\right) \tag{4}$$

$$\frac{\partial\vec{H}}{\partial t} = \nabla\times\vec{V}_f\times\vec{H} + \nu_m\nabla^2\vec{H} \tag{5}$$

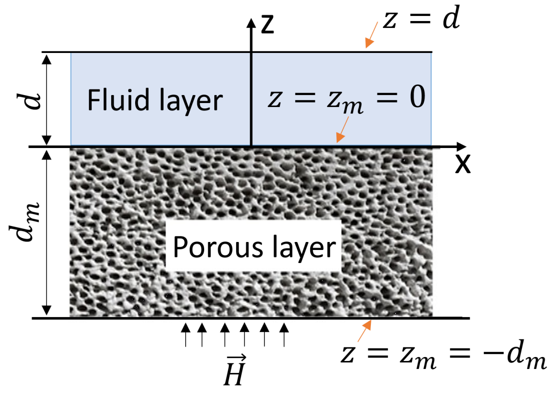

Figure 1. Geometry of the two-layer configuration.

2.2 porous medium

In the porous medium, $z \in (-d_m, 0)$, Eq. 6 up to Eq. 10

$$\nabla_m.\vec{V}_m = 0 \tag{6}$$

$$\nabla_m.\vec{H} = 0 \tag{7}$$

$$\frac{\rho_o}{\phi} + \frac{\partial\vec{V}_m}{\partial t_m} = -\nabla_m P_m - \frac{\mu}{K}\nabla_m\vec{V}_m + \mu_p\left(\vec{H}.\nabla_m\right)\vec{H} \tag{8}$$

$$A\frac{\partial T_m}{\partial t} + \left(\vec{V}_m.\nabla_m\right)T_m = \kappa_m\nabla_m^2 T_m + Q_2\left(T_m - T_o\right) \tag{9}$$

$$\phi\frac{\partial\vec{H}}{\partial t} = \nabla_m\times\vec{V}_m\times\vec{H} + \nu_{em}\nabla_m^2\vec{H} \tag{10}$$

Where $\vec{V}_f = (u_f, v_f, w_f)$ and $\vec{V}_m = (u_m, v_m, w_m)$ are velocity vectors, ρ_o is fluid density, μ is viscosity of the fluid, μ_p is magnetic permeability, P_f is pressure, ϕ porosity, K permeability, $A = \frac{(\rho_o C_p)_m}{(\rho_o C_p)_f}$ ratio of heat capacities, C_p specific heat, $\nu_m = \frac{1}{\mu_p\sigma_e}$ is magnetic viscosity, where σ_e electrical conductivity, κ_f and κ_m are thermal diffusivities, $\nu_{em} = \frac{\nu_m}{\phi}$ effective magnetic viscosity, T_f and T_m are temperatures, $\vec{H}$ is magnetic field, Q_1 and Q_2 are heat sources. (The subscripts f refer to the fluid domain and m refers to the porous domain).

Thus, the basic state is given by Eq. 11 up to Eq. 15 [25].

$$\left[\vec{V}_f, P_f, T_f, \vec{H}\right] = \left[0, P_{fb}(z), T_{fb}(z), H_o(z)\right] \tag{11}$$

$$\left[\vec{V}_m, P_m, T_m, \vec{H}\right] = \left[0, P_{mb}(z), T_{mb}(z), H_o(z)\right] \tag{12}$$

$$T_b(z) = T_o + \left[\frac{T_U - T_o}{sin\left(\sqrt{\frac{Q_1}{\kappa}}d\right)}\right]sin\left(\sqrt{\frac{Q_1}{\kappa}}z\right) \tag{13}$$

$$Where: \quad 0 \le z \le d$$

$$T_{mb}(z_m) = T_o + \left[\frac{T_o - T_L}{sin\left(\sqrt{\frac{Q_2}{\kappa_m}}d_m\right)}\right]sin\left(\sqrt{\frac{Q_2}{\kappa_m}}z_m\right) \tag{14}$$

$$Where: \quad -d_m \le z_m \le 0$$

$$T_o = \frac{T_U\sqrt{Q_1\kappa}\,sin\left(\frac{Q_2}{\kappa_m}d_m\right) + T_L\sqrt{Q_2\kappa_m}\,sin\left(\sqrt{\frac{Q_1}{\kappa}}d\right)}{\sqrt{Q_2\kappa_m}\,sin\left(\frac{Q_1}{\kappa}d\right) + \sqrt{Q_1\kappa}\,sin\left(\sqrt{\frac{Q_2}{\kappa_m}}d_m\right)} \tag{15}$$

Where T_o is the interface temperature and the subscript b representing basic state. We perturb the variables in the following form, Eqs. 16 and Eq. 17, to explore the stability of the fundamental solution.

$$\left[\vec{V}_f, P_f, T_f, \vec{H}\right] = \left[0, P_{fb}(z), T_{fb}(z), H_o(z)\right] + \\ + \left[\vec{V'}_f, P'_f, \theta_f, \vec{H'}\right] \tag{16}$$

$$\left[\vec{V}_m, P_m, T_m, \vec{H}\right] = \left[0, P_{mb}(z), T_{mb}(z), H_o(z_m)\right] + \\ + \left[\vec{V'}_m, P'_m, \theta_m, \vec{H'}\right] \tag{17}$$

3. Non-dimensional parameters

The variables are then non-dimensionalized by separate length scales so that each layer is of unit depth. They are as follows:

3.1 Fluid layer

In the fluid layer Eq. 18.

$$\left.\begin{aligned} &(u_f, v_f, w_f) = \frac{\kappa_f}{d}\left(u_f^*, v_f^*, w_f^*\right) \\ &\theta_f = (T_o - T_u)\,\theta^* \\ &(x, y, z) = d\,(x^*, y^*, z^*) \\ &t = \frac{d^2}{\kappa_f}t^* \\ &\nabla = \frac{1}{d}\nabla^* \end{aligned}\right\} \tag{18}$$

3.2 porous medium

In the porous layer Eq. 19

$$\left.\begin{aligned} &(u_m, v_m, w_m) = \frac{\kappa_m}{d_m}\left(u_m^*, v_m^*, w_m^*\right) \\ &\theta_m = (T_o - T_u)\,\theta_m^* \\ &(x_m, y_m, z_m) = d_m\,(x_m^*, y_m^*, z_m^*) \\ &t_m = \frac{d_m^2}{\kappa_m}t_m^* \\ &\nabla_m = \frac{1}{d_m}\nabla_m^* \end{aligned}\right\} \tag{19}$$

By introducing Eqs. 16, 17, 18 and 19 into the fundamental equations, simplifying them to a linear format, removing the pressure variable from the altered momentum equations through cross differentiation, and focusing solely on the vertical components. Thus, the following formulas are develop Eq. 20 up to Eq. 25.

$$\frac{1}{Pr_f}\frac{\partial(\nabla^2 w_f)}{\partial t} = \nabla^4 w_f + Q_f\tau_f\frac{\partial(\nabla^2 H_z)}{\partial z} \tag{20}$$

$$\frac{\partial\theta_f}{\partial t} - \frac{w_f\sqrt{R_I}}{sin\sqrt{R_I}}cos(\sqrt{R_I}z) = \nabla^2\theta_f + R_I\theta_f \tag{21}$$

$$\frac{\partial H_z}{\partial t} = \frac{\partial w_f}{\partial z} + \tau_f\nabla^2 H_z \tag{22}$$

$$\frac{\beta^2}{Pr_m}\frac{\partial(\nabla_m^2 w_m)}{\partial t} = -\nabla_m^2 w_m + Q_m\beta^2\tau_m\frac{\partial(\nabla_m^2 H_{zm})}{\partial z_m} \tag{23}$$

$$A\frac{\partial\theta_m}{\partial t_m}-\frac{w_m\sqrt{R_{Im}}}{sin\sqrt{R_{Im}}}cos(\sqrt{R_{Im}}z_m)=\nabla_m^2\theta_m+R_{Im}\theta_m \quad (24)$$

$$\phi\frac{\partial H_{zm}}{\partial t}=\frac{\partial w_m}{\partial z_m}+\tau_m\nabla_m^2H_{zm} \quad (25)$$

Here Pr_f and Pr_m are Prandtl numbers, W_f and w_m are vertical velocities, $\beta^2=Da$ is the Darcy number, $Q_f=\frac{\mu_pH_o^2d^2}{\mu\kappa_f\tau_f}$ and $Q_m=\frac{\mu_pH_o^2d_m^2}{\mu\kappa_m\tau_m}=\frac{Q_f\phi}{\zeta^2}$ are Chandrasekhar numbers, where $\zeta=\frac{d}{d_m}$ is the depth ratio, $\tau_f=\frac{\nu_m}{\kappa_f}$ and $\tau_m=\frac{\nu_{em}}{\kappa_m}$ are the diffusivity ratio, $R_I=\frac{q_fd^2}{\kappa_f}$ and $R_{Im}=\frac{q_md^2}{\kappa_m}$ are internal Rayleigh numbers. Nondimensionalizing the quantities by choosing separate scaling parameters for both layers, as considered by [25]. Then, to ascertain the state of marginal stability (oscillatory modes are not considered), normal mode analysis is implemented for the variables w_f, θ_f, H, and w_m, θ_m, H, Eq. 26 and 27.

$$[w_f,\theta_f,H]=[W_f(z),\Phi_f(z),H(z)]e^{i(lx+my)} \quad (26)$$

$$[w_m,\theta_m,H]=[W_m(z_m),\Phi_m(z_m),H(z_m)]e^{i(\tilde{l}x+\tilde{m}y)} \quad (27)$$

The resulting equations are Eqs. 28, 29, 30 and Eq. 31.

$$\left(D^2-a^2\right)^2W_f(z)-Q_fD^2W_f(z)=0 \quad (28)$$

$$\left(D^2-a^2+R_I\right)\Phi_f(z)+\frac{W_f(z)\sqrt{R_I}}{sin\sqrt{R_I}}cos(\sqrt{R_I}z) \quad (29)$$

$$\left(D^2-a^2\right)W_m(z_m)+Q_m\beta^2D_m^2W_m(z_m)=0 \quad (30)$$

$$\left(D^2-a^2+R_{Im}\right)\Phi_m(z)+\frac{W_m(z)\sqrt{R_{Im}}}{sin\sqrt{R_I}}cos(\sqrt{R_{Im}}z_m)=0 \quad (31)$$

Here $D=\frac{d}{dz}$ and $D_m=\frac{d}{dz_m}$ are differential operators, $a=\sqrt{l^2+m^2}$ and $a_m=\sqrt{\tilde{l}^2+\tilde{m}^2}$ are horizontal wave numbers. No-slip boundary conditions was incorporated as considered by [26]. The top free surface is assumed to be at constant heat flux, and the boundary conditions are Eq. 32 and Eq. 33.

$$W_f(1)=0,D\Phi_f(1)=0 \quad (32)$$

$$D^2W_f(1)+Ma_Ta^2\Phi_f(1)=0 \quad (33)$$

At the junction, the speed, perpendicular pressure, thermal energy, thermal flow, and lateral pressure are considered to be unbroken, and the constraints on the boundaries are Eq. 34.

$$\left.\begin{aligned}
&W_f(0)=\frac{\zeta}{\epsilon_T}W_m(0)\\
&\left(D^2+a^2\right)W_f(0)=\frac{\zeta}{\epsilon_T}\left(D_m^2+a_m^2\right)W_m(0)\\
&\left(D^3+3a^2D\right)W_f(0)=-\frac{\zeta^4}{Da\,\epsilon_T}D_mW_m(0)\\
&\Phi_f(0)=\frac{\epsilon_T}{\zeta}\Phi_m(0)\\
&D\Phi_f(0)=D_m\Phi_m(0)
\end{aligned}\right\} \quad (34)$$

The bottom rigid surface is either adiabatic or isother,mal to temperature and boundary conditions are Eq. 35.

$$\left.\begin{aligned}
&W_m(-1)=0\\
&D_m\Phi_m(-1)=0\\
&\Phi_m(-1)=0
\end{aligned}\right\} \quad (35)$$

Here $\epsilon_T=\frac{\kappa_f}{\kappa_m}$ is the thermal diffusivity ratio, $Ma_T=\frac{\partial\sigma}{\partial T_f}\frac{(T_O-T_u)d}{\mu\kappa_f}$ is the thermal Marangoni number, where is the surface tension.

4. Linear stability analysis and analytical solution procedure

The tMn is determined employing a closed form of solution for two unique thermal boundary scenarios, specifically: i) $(A-A)$, and ii) $(A-I)$.
The vertical velocities, $W_f(z)$ and $W_m(z_m)$, Eqs. 36 and E 37 are calculated by solving Eqs. 28 and 30 with boundary conditions Eqs. 32, 33, 34 and 35.

$$\begin{aligned}W_f(z)=A_1\left[cosh\left(\delta_1z\right)+\mathbb{F}_1\,sinh\left(\delta_1z\right)\right)+\\
+A_1\left(\mathbb{F}_2\,cosh\left(\delta_2z\right)+\mathbb{F}_3\,sinh\left(\delta_2z\right)\right]\end{aligned} \quad (36)$$

$$W_m(z_m)=A_1\left[\mathbb{F}_{m1}\,cosh\left(\delta_mz_m+\right)\mathbb{F}_{m2}\,sinh\left(\delta_mz_m\right)\right] \quad (37)$$

The constants that are obtained from the above-considered boundary conditions are listed in Appendix A. Furthermore, The perturbed temperature distributions for A-A are Eqs. 38 and 39

$$\Phi_{f1}(z)=A_1\left[N_1\,cosh(bz)+N_2\,sinh(bz)-\Pi_1(z)\right] \quad (38)$$

$$\Phi_{m1}(z)=A_1\left[N_3\,cosh(b_mz_m)+N_4\,sinh(b_mz_m)-\Pi_2(z_m)\right] \quad (39)$$

where the key terms are listed in appendix-B. Then, introducing Eq. 33 to obtain Marangoni numbers Ma_{T1}, Eq. 40.

$$Ma_{T1}=-\frac{\delta_1^2\left[cosh\,\delta_1+\mathbb{F}_1\,sinh\,\delta_1\right]+\delta_2^2\left[\mathbb{F}_2\,cosh\,\delta_2+\mathbb{F}_3\,sinh\,\delta_2\right]}{a^2\left[N_1\,cosh\,b+N_2\,sinh\,b-\Pi_1(1)\right]} \quad (40)$$

The perturbed temperature distributions for $A-I$, Eqs. 41 and 42.

$$\Phi_{f2}=A_1\left[B_1\,cosh\,(bz)+B_2\,sinh\,(bz)-\Pi_1(z)\right] \quad (41)$$

$$\Phi_{m2}(z_m)=A_1\left[B_3\,cosh\,(b_mz_m)+B_4\,sinh\,(b_mz_m)-\Pi_2(z_m)\right] \quad (42)$$

Introducing Eq. 33 to the Eqs. 40 and 42 the Marangoni number Ma_{T2} obtained as Eq. 43.

$$Ma_{T2}=-\frac{\delta_1^2\left[cosh\,\delta_1+\mathbb{F}_1\,sinh\,\delta_1\right]+\delta_2^2\left[\mathbb{F}_2\,cosh\,\delta_2+\mathbb{F}_3\,sinh\,\delta_2\right]}{a^2\left[B_1\,cosh\,b+B_2\,sinh\,b-\Pi_1(1)\right]} \quad (43)$$

The constants N_i and B_i are obtained using appropriate thermal boundary conditions are listed in Appendix-C, where $i=1,2,3,\ and\ 4$.

5. Results and Discussion

In this study, we investigate the $Marangoni$ magneto-convection within a composite fluid-saturated isotropic porous medium, incorporating the effects of internal heat sources. The system is analyzed under two distinct thermal boundary conditions: (i) both boundaries thermally conducting (A–A), and (ii) one conducting and one insulating (A–I). An exact analytical method is employed to determine the marginal stability threshold (tMn). The influence of various physical parameters, including magnetic field strength, $Marangoni$ number, Darcy number, and internal heat generation on tMn is examined. Results are presented graphically as functions of the depth ratio, and the impact of the chosen boundary conditions on the onset of convection is thoroughly discussed. The tMns, for A-A and for A-I, are compared in Fig. 2. The physical parameters considered are refer Table 1. The graph reveals that initially there is no difference between the two thermal boundaries, but as increases, the tMn decreases, whereas increases. Thus, the system is more stable for (A-I) temperature conditions and most unstable for (A-A) temperature conditions. In the (A-I) configuration, the isothermal lower boundary acts as an efficient thermal sink, suppressing temperature perturbations in spite of the presence of internal heat sources. Combined with magnetic damping, this stabilizing effect becomes stronger as the depth ratio increases, thereby delaying the onset of Marangoni convection. In case of (A-A), the increasing depth ratio enlarges the fluid layer, allowing greater accumulation of internally generated heat due to the absence of thermal dissipation. This absence enhances and amplifies temperature perturbations and strengthens surface-tension gradients at the free surface, overcoming magnetic damping. Consequently, the composite system is destabilized, and the onset of MMC occurs faster. The effects of Darcy number on tMns and are depicted in Fig. 3. Increasing the values of, the tMns, and decreases, showing a destabilizing effect and hence the onset of MMC is augmented. Even though (A-A) and (A-I) behave differently with respect to depth ratio, the permeability effect acts through hydrodynamics, so it destabilizes the system in both cases.

Table 1. The range of parameters considered in the present work.

Symbol	Definition	Physical Meaning	Range
a	Horizontal wave number	⇒ Horizontal size of convection cells.	0–2.5
R_I	Internal Rayleigh number in the fluid layer	⇒ Strength of the heat source in the fluid layer.	0 – 1
R_{I_m}	Internal Rayleigh number in the porous layer	⇒ Strength of the heat source in the porous layer.	0 – 1
Ma_T	Thermal Marangoni number	⇒ Ratio of surface tension forces to viscous forces.	Dependent
ϵ_T	Thermal diffusivity ratio	⇒ Ratio of thermal diffusivity in the fluid layer to porous layer.	0 – 1
Da	Darcy number	⇒ Measures permeability of porous medium relative to layer thickness; indicates porous resistance.	0 – 1
Q_f	Chandrasekhar number	⇒ Strength of applied magnetic field; ratio of magnetic to viscous forces.	$0 - 10^3$
ζ	Depth ratio	⇒ Ratio of fluid layer thickness to porous layer thickness.	0 ⇒ Any value. > 1 ⇒ Fluid layer dominant < 1 ⇒ Porous layer dominant = 1 ⇒ Both layers are of equal depth

Further, the diverging curves in Fig. 3 for greater values also suggest that this parameter is important in the fluid layer dominant composite system.

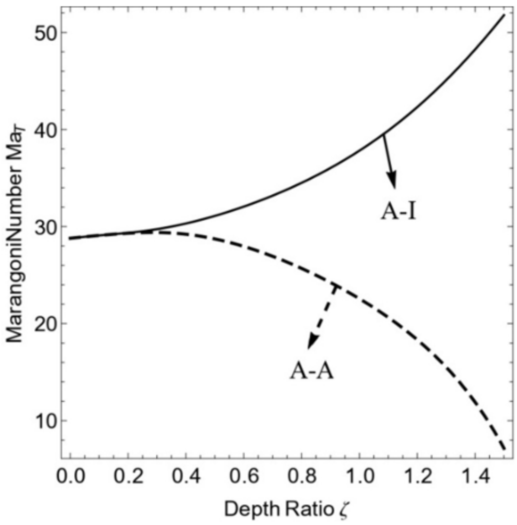

Figure 2. Comparison of Adiabatic–Adiabatic and Adiabatic–Isothermal boundary conditions.

The consequences of are seen in Fig. 4. The tMns, and drop as increases, causing the system to become unstable and hastening the onset of MMC. This is because the internal heat source parameter boosts the overall temperature of the system, causing instability to occur. The tMns and with respect to computed for are shown in Fig. 5 respectively. According to the graphs, has the effect of destabilizing the system, signifying that the onset of MMC happens faster. The curves in the instance of A-A are diverging at increasing values of, showing that this parameter is crucial in fluid layer dominant system. In the case of A-I, the influence is uniform across both layers. Figure 6, respectively, displays the implications for the thermal boundaries, A-A and A-I. Varying the $tMns$, and increasing the system stability. The effect of is to suppress the onset of MMC. In case of (A-A), as seen in Fig. 6a, the curves are converging with an increase in the depth ratio. This indicates that the effect of the Chandrasekhar number is more pronounced in the porous-layer-dominant composite system. While in curves change proportionately with respect to the depth ratio in the case of (A-I). Varying the parameter, as illustrated in Fig. 7, a dual impact is noticed in the case of A-A. That is, it destabilizes the system in the porous dominant zone and stabilizes the system in the fluid dominant region. As a result, the depth ratio has a substantial impact on the system's stability. The observed dual behavior arises from a shift in the thermal control between the porous and fluid layers, governed by the depth ratio, internal heating, and magnetic damping. In the case of A-I, this parameter has a destabilizing effect on the system since the tMn, decreases with increasing, and the MMC is accelerated. The impact of horizontal wave number on and is observed in Fig. 8. As a increases, both Ma_{T1} and Ma_{T2} increase, indicating a stabilizing effect and hence the onset of MMC is delayed.

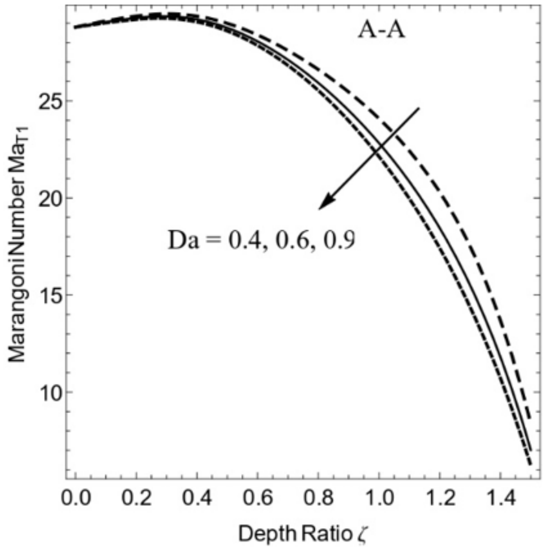

(a) Model 01- Adiabatic-Adiabatic

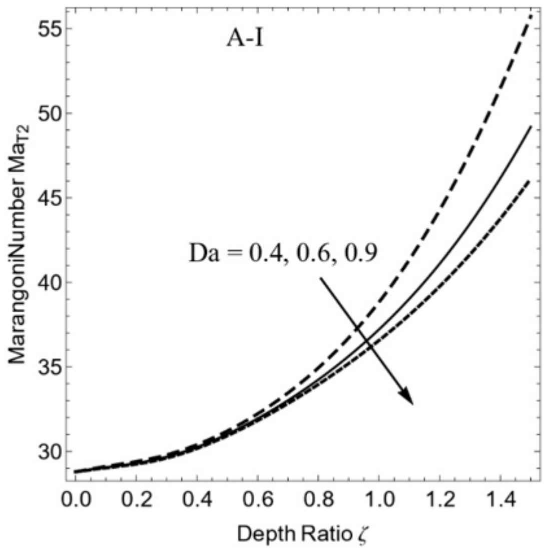

(b) Model 02- Adiabatic-Isothermal

Figure 3. The variation of Darcy number on tMn.

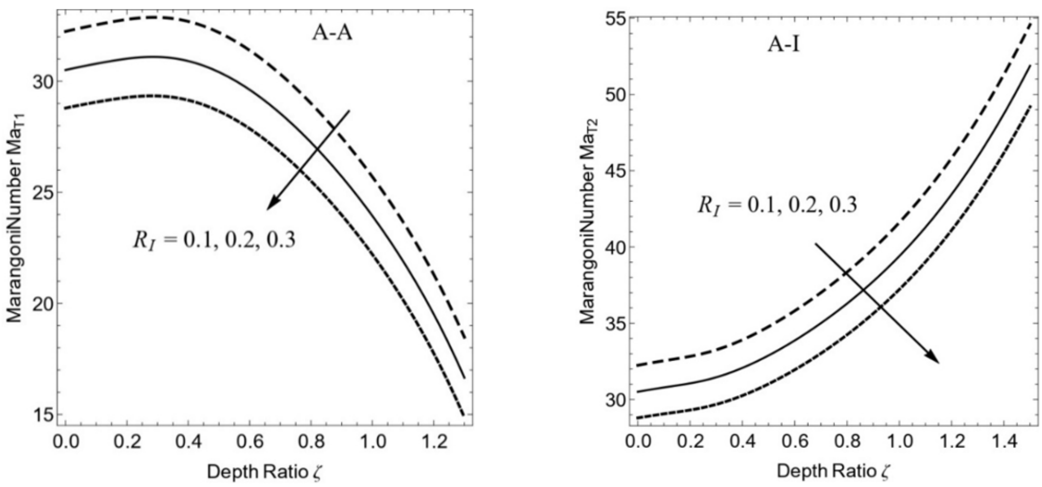

(a) Model 01- Adiabatic-Adiabatic

(b) Model 02- Adiabatic-Isothermal

Figure 4. The impacts of modified internal Rayleigh number (fluid region) on tMn.

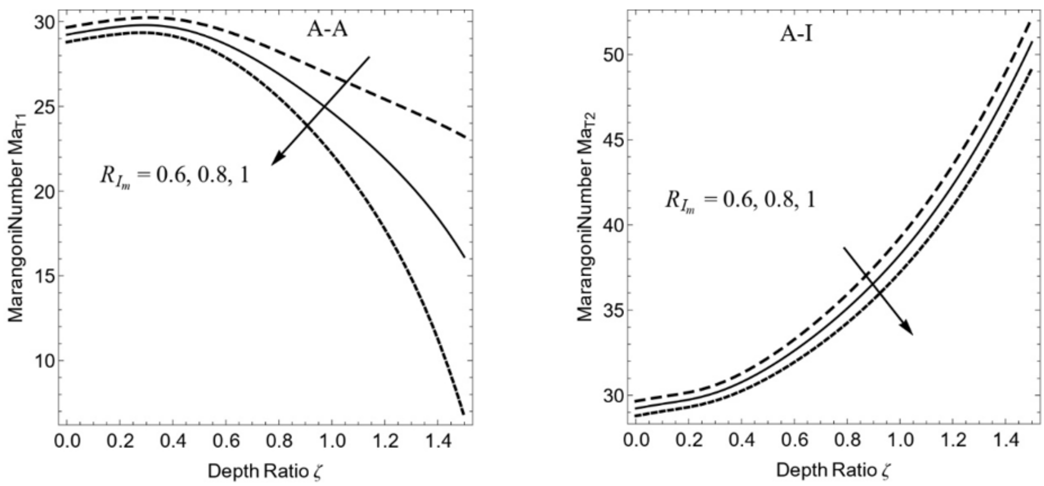

(a) Model 01- Adiabatic-Adiabatic

(b) Model 02- Adiabatic-Isothermal

Figure 5. The variation of modified internal Rayleigh number (porous region) on tMn.

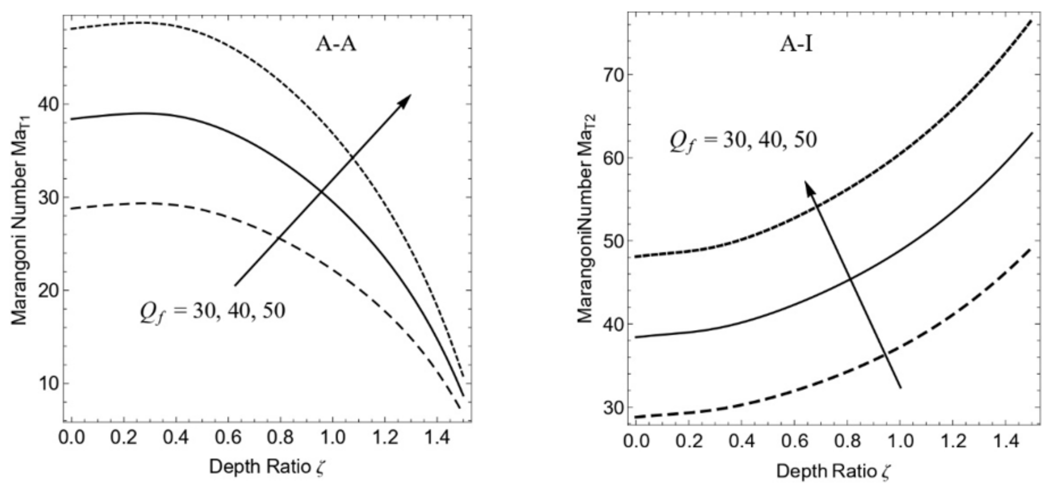

(a) Model 01- Adiabatic-Adiabatic

(b) Model 02- Adiabatic-Isothermal

Figure 6. The variation of Chandrasekhar number on tMn.

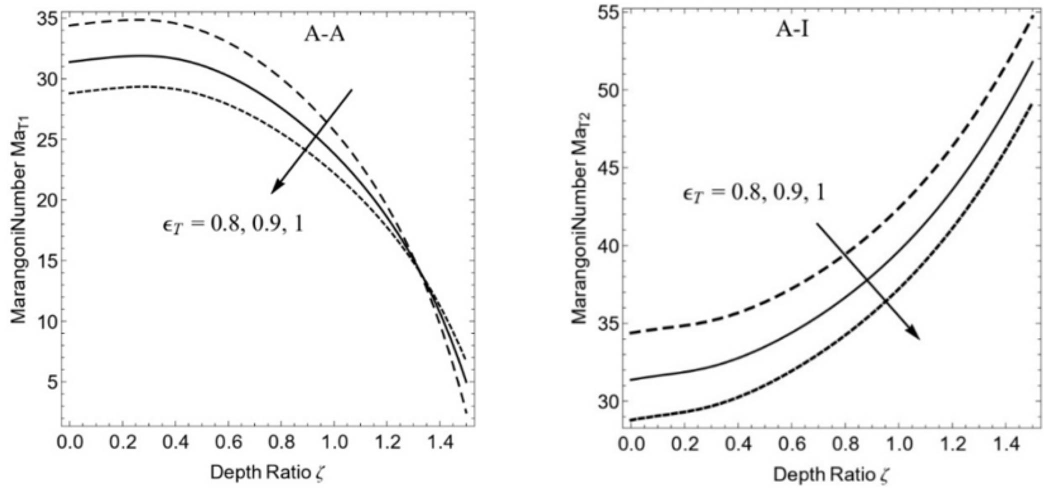

(a) Model 01- Adiabatic-Adiabatic

(b) Model 02- Adiabatic-Isothermal

Figure 7. The effects of thermal diffusivity ratio on tMn.

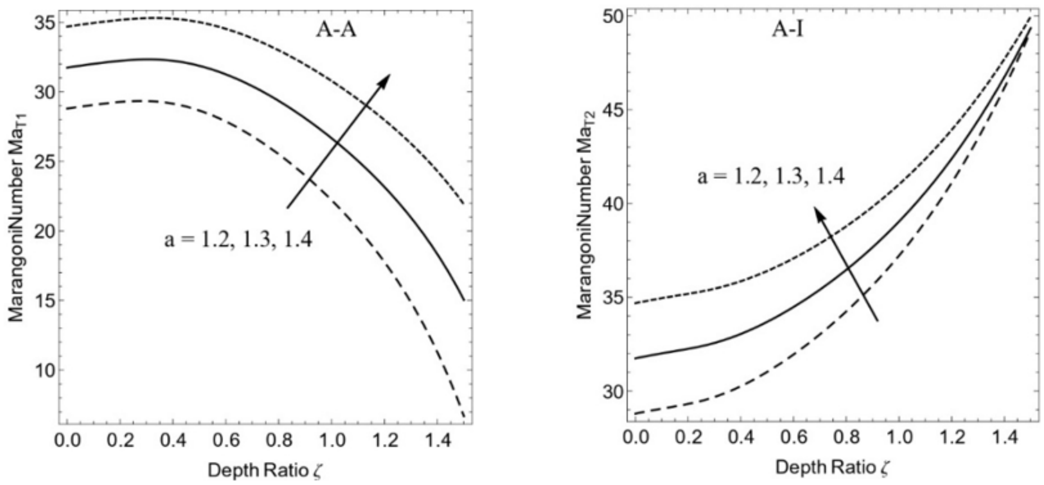

(a) Model 01- Adiabatic-Adiabatic

(b) Model 02- Adiabatic-Isothermal

Figure 8. Variation of thermal Marangoni number with horizontal wave number.

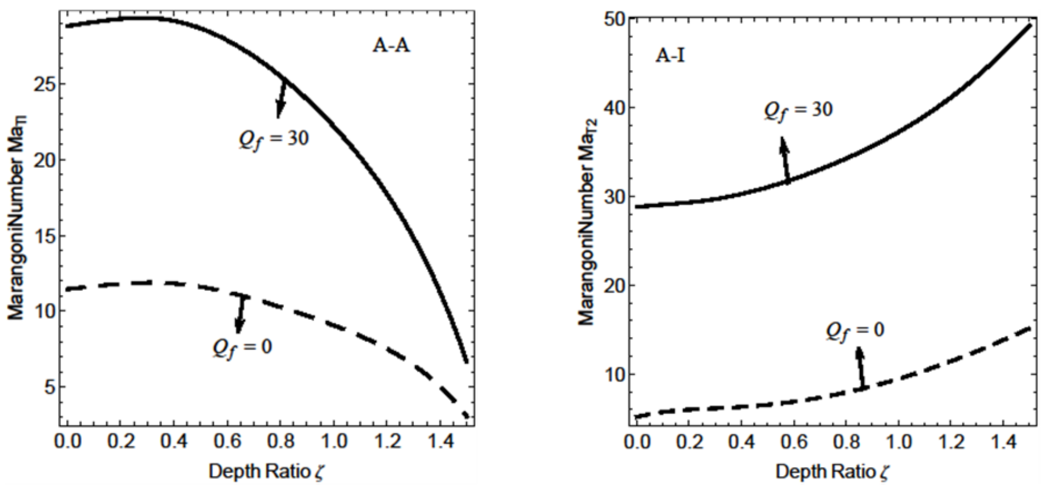

(a) Model 01- Adiabatic-Adiabatic

(b) Model 02- Adiabatic-Isothermal

Figure 9. Comparison between thermal boundaries with Chandrasekhar number (present work and without Chandrasekhar number from [14])

6. Validation

It is important to mention that without a magnetic field, the results are consistent with the findings of [14].

7. Conclusion

The detailed investigation into the stability of Marangoni Magneto-convective (MMC) flow is conducted within the framework of a dual-layer system. The analysis considers the effects of variable heat sources, a pervasive magnetic field, varying depth ratios, and thermal boundaries. In this fascinating setup, the upper layer of the fluid remains unconfined and free, allowing for convection flow driven by surface tension forces. In contrast, the lower porous layer exhibits rigidity and immobility. To further unravel the thermal dynamics involved, we examine two unique thermal boundary conditions: i) both boundaries are kept at a constant heat flux (Adiabatic-Adiabatic (A-A)), and ii) the upper surface is adiabatic while the lower surface is maintained at a constant temperature i.e., the Adiabatic-Isothermal (A-I). For both the boundaries, closed form of solutions are obtained. From the graphical results, the following conclusions are drawn.

- The composite system is most stable in case of A-I thermal boundaries, i.e., upper free adiabatic surface and lower rigid isothermal surface and less stable in case of A-A, i.e., both the surfaces are adiabatic.
- The effects of internal Rayleigh numbers, and destabilize the system. The onset of MMC is faster, as the internal heat source parameter boosts the overall temperature of the system, causing instability to occur.
- The Chandrasekhar number, has a stabilizing effect on the system for both types of thermal boundaries. The imposition of a magnetic field suppresses the onset of MMC.
- The onset of MMC can be accelerated or delayed by selecting an appropriate depth ratio and thermal boundaries for the parameter.

Authors' contribution

Sumithra R: Writing - Review & Editing, Formal analysis; Archana M. A: Investigation, Conceptualization; Manjunatha N: Writing - Review & Editing, Methodology, Validation; Khaled Al-Farhany: Investigation, validation; Shankara: Investigation, Conceptualization; Vijaya Kumar: Writing - Review & Editing, Writing - Original Draft.

Declaration of competing interest

The authors declare no conflicts of interest.

Funding source

This research received no specific grant from any funding.

Data availability

The data that support the findings of this study are available from the corresponding author upon reasonable request.

Acknowledgements

The authors would like to acknowledge the anonymous reviewers and editors of the journal.

A. Appendix Section

A.1 Related to Eqs. 30-37

The constants are:

$$\delta_1 = \frac{\sqrt{Q_f} + \sqrt{Q_f + 4a^2}}{2} \qquad \text{(A1.1)}$$

$$\delta_2 = \frac{\sqrt{Q_f} - \sqrt{Q_f + 4a^2}}{2} \qquad \text{(A1.2)}$$

$$\delta_m = \frac{a_m}{\sqrt{1 + Q_f \beta^2}} \qquad \text{(A1.3)}$$

$$\mathbb{F}_1 = \frac{A_2 \mathbb{F}_{m2}\, sinh\ \delta_2 - A_4 \left[cosh\ \delta_1 + \mathbb{F}_2\, cosh\ \delta_2\right]}{A_4\, sinh\ \delta_1 - A_3\, sinh\ \delta_2} \qquad \text{(A1.4)}$$

$$\mathbb{F}_{m1} = \frac{\epsilon_T}{\zeta}\left(1 + \mathbb{F}_2\right) \qquad \text{(A1.5)}$$

$$\mathbb{F}_{m2} = \mathbb{F}_{m1} coth\ \delta_m \qquad \text{(A1.6)}$$

$$\mathbb{F}_2 = \frac{\zeta^2\left(\delta_m^2 + a_m^2\right) - \left(\delta_1^2 + a^2\right)}{\left(\delta_2^2 + a^2\right) - \zeta^2\left(\delta_m^2 + a_m^2\right)} \qquad \text{(A1.7)}$$

$$\mathbb{F}_3 = -\frac{1}{A_4}\left(A_2 \mathbb{F}_{m2} + \mathbb{F}_1 A_3\right) \qquad \text{(A1.8)}$$

$$A_2 = \frac{\delta_m \zeta^4}{\epsilon_T\, Da} \qquad \text{(A1.9)}$$

$$A_3 = \delta_1^3 - 3a^2 \delta_1 \qquad \text{(A1.10)}$$

$$A_4 = \delta_2^3 - 3a^2 \delta_2 \qquad \text{(A1.11)}$$

A.2 Related to Eq. 40

The constants are:

$$\Pi_1(z) = \frac{\sqrt{R_I}}{sin\sqrt{R_I}}\left[\hbar_{f1}(\gamma_1 + \gamma_2) + \hbar_{f2}(\gamma_3 + \gamma_4)\right] \qquad \text{(A2.1)}$$

$$\Pi_2(z_m) = \frac{\hbar\sqrt{R_{Im}}}{sin\sqrt{R_I m}}\left(\gamma_5 + \gamma_6\right) \qquad \text{(A2.2)}$$

$$b = \sqrt{a^2 - R_I} \qquad \text{(A2.3)}$$

$$b_m = \sqrt{a_m^2 - R_{Im}} \qquad \text{(A2.4)}$$

$$\gamma_1 = \hbar\, cos\left(\sqrt{R_I z}\right)\left[cosh\ (\delta_1 z) + \mathbb{F}_1\ sinh(\delta_1 z)\right] \qquad \text{(A2.5)}$$

$$\gamma_2 = \hbar\, cos\left(\sqrt{R_I z}\right)\left[\mathbb{F}_2 cosh\ (\delta_2 z) + \mathbb{F}_3 3\ sinh(\delta_2 z)\right] \qquad \text{(A2.6)}$$

$$\gamma_3 = 2\sqrt{R_I}\delta_1\ sin(\sqrt{R_I z})\left[sinh(\delta_1 z) + \mathbb{F}_1 cosh\ (\delta_1 z)\right] \qquad \text{(A2.7)}$$

$$\gamma_4 = 2\sqrt{R_I}\delta_2\ sin(\sqrt{R_I z})\left[\mathbb{F}_2 sinh(\delta_2 z) + \mathbb{F}_3 cosh\ (\delta_2 z)\right] \qquad \text{(A2.8)}$$

$$\gamma_5 = \hbar\, cos(\sqrt{R_{Im} z_m})\left[\mathbb{F}_{m1} cosh(\delta_m z_m) + \mathbb{F}_{m2} sinh\ (\delta_m z_m)\right] \qquad \text{(A2.9)}$$

$$\gamma_6 = 2\sqrt{R_{Im}}\delta_m\ sin(\sqrt{R_{Im} z_m}) \left[\mathbb{F}_{m1} sinh(\delta_m z_m) + \mathbb{F}_{m2} cosh\ (\delta_m z_m)\right] \qquad \text{(A2.10)}$$

$$N_1 = \Lambda_2 + \frac{\epsilon_T}{\zeta} N_3 \qquad \text{(A2.11)}$$

$$N_2 = \frac{\Lambda_1 - N_1 b\ sinh\ b}{b\ cosh\ b} \qquad \text{(A2.12)}$$

$$\varrho_1 = \delta_1^2 - a^2 \qquad \text{(A2.13)}$$

$$N_3 = \frac{(\Lambda_1 - b\Lambda_2\ sinh\ b)\, cosh\ b_m - (\Lambda_3 cosh\ b_m + \Lambda_4)\, cosh\ b}{b_m sinh\ b_m\ cosh\ b + b\frac{\epsilon_T}{\zeta} sinh\ b\ cosh\ b_m} \qquad \text{(A2.14)}$$

$$N_4 = \frac{N_2 b - \Lambda_3}{b_m} \qquad \text{(A2.15)}$$

$$\varrho_2 = \delta_2^2 - a^2 \qquad \text{(A2.16)}$$

$$\varrho_{f1} = \frac{1}{\varrho_1^2 + 4R_1\delta_1^2} \qquad \text{(A2.17)}$$

$$\varrho_{f2} = \frac{1}{\varrho_2^2 + 4R_1\delta_2^2} \qquad \text{(A2.18)}$$

$$\varrho_m = \frac{1}{\varrho_3^2 + 4R_{1m}\delta_m^2} \qquad \text{(A2.19)}$$

$$\varrho_3 = \delta_m^2 - a_m^2 \qquad \text{(A2.20)}$$

$$\Lambda_{32} = \varrho_m F_{m2}\delta_m\left(\varrho_3 + 2R_{Im}\right) \qquad \text{(A2.21)}$$

$$\Lambda_3 = \frac{\sqrt{R_I}}{sin\sqrt{R_I}}\Lambda_{31} - \frac{\sqrt{R_{Im}}}{sin\sqrt{R_{Im}}}\Lambda_{32} \qquad \text{(A2.22)}$$

$$\Lambda_{31} = \varrho_{f1} F_1 \delta_1 \left(\varrho_1 + 2R_I\right) + \varrho_{f2} F_3 \delta_2 \left(\varrho_2 + 2R_I\right) \tag{A2.23}$$

$$\Lambda_1 = \frac{\sqrt{R_I}}{sin\sqrt{R_I}}\left[\varrho_{f1}\left\{\varrho_1\Lambda_{11} + 2\sqrt{R_I}\,\delta_I\Lambda_{12}\right\}\right] + \\ + \frac{\sqrt{R_I}}{sin\sqrt{R_I}}\left[\varrho_{f2}\left\{\varrho_2\Lambda_{13} + 2\sqrt{R_I}\,\delta_2\Lambda_{14}\right\}\right] \tag{A2.24}$$

$$\Lambda_2 = \frac{\sqrt{R_I}}{sin\sqrt{R_I}}\left[\varrho_{f1}\varrho_1 + F_2\varrho_2\varrho_{f2}\right] - \varrho_m\frac{F_{m1}\,\epsilon_T\,\varrho_3\sqrt{R_{Im}}}{\zeta\, sin\sqrt{R_{Im}}} \tag{A2.25}$$

$$\Lambda_4 = \frac{\varrho_m\sqrt{R_{Im}}}{sin\sqrt{R_I}}\left[\Lambda_{41} + \Lambda_{42} + \Lambda_{43}\right] \tag{A2.26}$$

$$\Lambda_{41} = \delta_m\varrho_3 cos\sqrt{R_{Im}}\left[F_{m1}sinh\delta_m + F_{m2}cosh\delta_m\right] \tag{A2.27}$$

$$\Lambda_{42} = \sqrt{R_{Im}}\left(\delta_m^2 + a_m^2\left(\left[F_{m2}sinh\delta_m + F_{m1}cosh\delta_m\right]\right.\right. \tag{A2.28}$$

$$\Lambda_{43} = 2R_{Im}\delta_m cos\sqrt{R_{Im}}\left[F_{m2}cosh\delta_m - F_{m1}sinh\delta_m\right] \tag{A2.29}$$

$$\Lambda_{11} = \delta_1 cos\sqrt{R_I}\left[sinh\delta_1 + F_1 cosh\delta_1\right] - \\ - \sqrt{R_I}sin\sqrt{R_I}\left[cosh\delta_1 + F_1 sinh\delta_1\right] \tag{A2.30}$$

$$\Lambda_{12} = \delta_1 sin\sqrt{R_I}\left[cosh\delta_1 + F_1 sinh\delta_1\right] + \\ + \sqrt{R_I}cos\sqrt{R_I}\left[sinh\delta_1 + F_1 cosh\delta_1\right] \tag{A2.31}$$

$$\Lambda_{13} = \delta_2 cos\sqrt{R_I}\left[F_2 sinh\delta_2 + F_3 cosh\delta_2\right] - \\ - \sqrt{R_I}sin\sqrt{R_I}\left[F_2 cosh\delta_2 + F_3 sinh\delta_2\right] \tag{A2.32}$$

$$\Lambda_{14} = \delta_2 sin\sqrt{R_I}\left[F_2 cosh\delta_2 + F_3 sinh\delta_2\right] + \\ + \sqrt{R_I}cos\sqrt{R_I}\left[F_2 sinh\delta_2 + F_3 cosh\delta_2\right] \tag{A2.33}$$

A.3 Related to Eq. 40

The constants are:

$$B_1 = \Lambda_2 + \frac{\epsilon_T}{\zeta} \tag{A3.1}$$

$$B_2 = \frac{\Lambda_1 - B_3 b sinhb}{bcoshb} \tag{A3.2}$$

$$B_3 = \frac{\left(\Lambda - b\Lambda_2 sinhb\right)sinhb_m - \left(\Lambda_3 sinhb_m - \Gamma_4 b_m\right)coshb}{b_m cohbcoshb_m + b\frac{\epsilon_T}{\zeta}sinhbsinhb_m} \tag{A3.3}$$

$$B_4 = \frac{c_{f4}b - \Lambda}{b_m} \tag{A3.4}$$

$$\Gamma_4 = \varrho_m\frac{\sqrt{R_{Im}}}{sin\sqrt{R_{Im}}}\left(\Gamma_{41+\Gamma_{42}}\right) \tag{A3.5}$$

$$\Gamma_{41} = \varrho_3 cos\sqrt{R_{Im}}\left(F_{m1}cosh\delta_m - F_{m2}sinh\delta_m\right) \tag{A3.6}$$

$$\Gamma_{42} = \sqrt{R_{Im}}sin\sqrt{R_{Im}}\left(F_{m1}sinh\delta_m - F_{m2}cosh\delta_m\right) \tag{A3.7}$$

REFERENCES

[1] M. Z. Saghir, P. Comi, and M. Mehrvar, "Effects of interaction between rayleigh and marangoni convection in superposed fluid and porous layers," *International Journal of Thermal Sciences*, vol. 41, no. 3, pp. 207–215, 2002. [Online]. Available: https://doi.org/10.1016/S1290-0729(01)01309-6

[2] R. Kozak, M. Z. Saghir, and A. Viviani, "Marangoni convection in a liquid layer overlying a porous layer with evaporation at the free surface," *Acta Astronautica*, vol. 55, no. 3-9, pp. 189–197, 2004. [Online]. Available: https://doi.org/10.1016/j.actaastro.2004.05.017

[3] I. S. Shivakumara, C. E. Nanjundappa, and K. B. Chavaraddi, "Darcy-benard-marangoni convection in porous media," *International Journal of Heat and Mass Transfer*, vol. 52, no. 11-12, pp. 2815–2823, 2009. [Online]. Available: https://doi.org/10.1016/j.ijheatmasstransfer.2008.09.038

[4] G. B. McFadden, S. R. Coriell, K. Gurski, and D. Cotrell, "Onset of convection in two liquid layers with phase change," *Physics of Fluids*, vol. 19, no. 10, p. 104109, 2007. [Online]. Available: https://doi.org/10.1063/1.2800339

[5] N. Manjunatha, R. Sumithra, and R. K. Vanishree, "Darcy-benard double diffusive marangoni convection in a composite layer system with constant heat source along with non-uniform temperature gradients," *Malaysian Journal of Fundamental and Applied Sciences*, vol. 17, no. 1, pp. 7–15, 2021. [Online]. Available: https://doi.org/10.11113/MJFAS.V17N1.1984

[6] R. Sumithra, S. Venkatraman, H. Aldeeb, N. B. Patil, S. Singh, N. Manjunatha, and R. J. Punith Gowda, "The onset of magneto–darcy–rayleigh–bénard convection under local thermal non-equilibrium with two-layer system," *Modern Physics Letters B*, vol. 39, no. 22, p. 2550067, 2025. [Online]. Available: https://doi.org/10.1142/s0217984925500678

[7] R. Sumithra and S. Venkatraman, "Local thermal non-equilibrium dominant darcy-rayleigh-benard-magneto-marangoni convection in a composite layer," *Journal of Mines, Metals and Fuels*, vol. 70, no. 7A, pp. 1–12, 2022. [Online]. Available: https://doi.org/10.18311/jmmf/2022/31853

[8] M.-I. Char and K.-T. Chiang, "Stability analysis of benard-marangoni convection in fluids with internal heat generation," *Journal of Physics D: Applied Physics*, vol. 27, no. 4, pp. 748–755, 1994.

[9] M.-I. Char, K.-T. Chiang, and J. J. Jou, "Oscillatory instability analysis of bénard–marangoni convection in a rotating fluid with internal heat generation," *International Journal of Heat and Mass Transfer*, vol. 40, no. 4, pp. 857–867, 1997.

[10] N. M. Mokhtar, N. M. Arifin, R. Nazar, F. Ismail, and M. Suleiman, "Effect of internal heat generation on marangoni convection in a fluid saturated porous medium," *International Journal of Applied Mathematics & Statistics*, vol. 19, no. D10, pp. 111–122, 2010.

[11] N. Mokhtar, M. Arifin, R. Nazar, F. Ismail, and M. Suleiman, "Effect of internal heat generation on marangoni convection in a superposed fluid-porous layer with deformable free surface," *International Journal of Physical Sciences*, vol. 6, no. 23, pp. 5550–5563, 2011.

[12] I. S. Shivakumara, S. P. Suma, R. Indira, and Y. H. Gangadharaiah, "Effect of internal heat generation on the onset of marangoni convection in a fluid layer overlying a layer of an anisotropic porous medium," *Transport in Porous Media*, vol. 92, no. 3, pp. 727–743, 2012.

[13] Y. H. Gangadharaiah, "Darcy–benard–marangoni ferroconvection with internal heat generation," *Journal of Global Research in Mathematical Archives*, vol. 1, no. 6, pp. 01–13, 2013.

[14] R. Sumithra, M. A. Archana, and R. K. Vanishree, "Darcy-benard surface tension driven convection in a composite layer with temperature dependent heat source," *Malaya Journal of Matematik*, vol. 8, no. 4, pp. 2074–2081, 2020.

[15] N. Manjunatha, R. Sumithra, K. M. Yogeesha, R. Kumar, and R. N. Kumar, "Roles and impacts of heat source/sink and magnetic field on non-darcy three-component marangoni convection in a two-layer structure," *International Journal of Modern Physics B*, vol. 37, no. 19, p. 2350186, 2023. [Online]. Available: https://doi.org/10.1142/s0217979223501862

[16] S. Chandrasekhar and J. Gillis, *Hydrodynamic and Hydromagnetic Stability*, 1962.

[17] N. Rudraiah and G. N. Sekhar, "Convection in magnetic fluids with internal heat generation," *Journal of Heat Transfer*, vol. 113, no. 1, pp. 122–127, 1991.

[18] S. K. Wilson, "The effect of a uniform magnetic field on the onset of steady bénard-marangoni convection in a layer of conducting fluid," *Journal of Engineering Mathematics*, vol. 27, pp. 161–188, 1993.

[19] Q. Liu and A. Wang, "Instability of two-layer marangoni-bénard convection with high-frequency vibration," *Journal of Beijing Jiaotong University*, vol. 30, no. 4, pp. 1–6, 2006. [Online]. Available: https://doi.org/10.3969/j.issn.1673-0291.2006.04.002

[20] H. M. Banjer and A. Abdullah, "Thermal instability of a two-layer system in the presence of magnetic field," in *International Conference on Mathematical Methods, Computational Techniques and Intelligent Systems*, 2010, pp. 21–29.

[21] T. Tagawa, "Magnetic bénard-marangoni convection in an annular liquid layer," *Transactions of the Japan Society of Mechanical Engineers B*, vol. 78, no. 787, pp. 618–633, 2012. [Online]. Available: https://doi.org/10.1299/KIKAIB.78.618

[22] M. Celli, P. Vayssiere Brandão, L. S. de B. Alves, and A. Barletta, "Convective instability in a darcy flow heated from below with internal heat generation," *Transport in Porous Media*, vol. 112, no. 3, pp. 563–575, 2016. [Online]. Available: https://doi.org/10.1007/S11242-016-0658-2

[23] T. Lyubimova and Y. Parshakova, "Onset of thermal buoyancy convection in a two-layer system with deformable interface and fixed heat flux at the boundaries under terrestrial and microgravity conditions," *Microgravity Science and Technology*, vol. 32, no. 3, pp. 295–304, 2020. [Online]. Available: https://doi.org/10.1007/S12217-019-09772-0

[24] S. Bhavya and C. E. Nanjundappa, "Energy based volumetric internal heating on bénard-marangoni ftc in a ferrofluid-porous saturated layer: effects of mfd viscosity and thermal bounded surfaces," *International Journal of Applied Engineering Research*, vol. 17, no. 1, pp. 21–29, 2022. [Online]. Available: https://doi.org/10.37622/ijaer/17.1.2022.21-29

[25] Yellamma, N. Manjunatha, R. Udhayakumar, J. A. Barakah, R. Sumithra, and E. Ahmed, "The impact of heat source and temperature gradient on brinkman-bènard triple-diffusive magneto-marangoni convection in a two-layer system," *Symmetry*, vol. 15, no. 3, p. 644, 2023. [Online]. Available: https://doi.org/10.3390/sym15030644

[26] T. Boeck, "Stability analysis of wall-attached bénard–marangoni convection in a vertical magnetic field," *Proceedings in Applied Mathematics and Mechanics*, vol. 23, p. e202300020, 2023.

[27] M. N. M. Fadzil and I. Ibrahim, "The marginal stability of oscillatory bénard-marangoni convection with internal heat generation," *Journal of Computing Research and Innovation (JCRINN)*, vol. 8, no. 2, 2023. [Online]. Available: https://doi.org/10.24191/jcrinn.v8i2.342

[28] R. Moussa, H. Lagziri, F. El Khanoussi, and H. El Fakiri, "The effects of heterogeneity on darcy-benard convection saturated with a ferrofluid," *E3S Web of Conferences*, vol. 601, p. 00095, 2025. [Online]. Available: https://doi.org/10.1051/e3sconf/202560100095

How to cite this article:
Sumithra R., Archana M. A., Manjunatha N., Khaled Al-Farhany, Shankara and Vijaya Kumar (2026). 'Stability analysis of marangoni magneto-convective flow with heat generation: effects of depth ratio and thermal boundaries', Al-Qadisiyah Journal for Engineering Sciences, 19(2), pp. 231- 240. https://doi.org/10.30772/qjes.2026.166109.1780